THE ASTROPHYSICAL JOURNAL, 222:342–356, 1978 May 15

6 CENTIMETER OBSERVATIONS OF SOLAR BURSTS WITH 6″ RESOLUTION

C. E. ALISSANDRAKIS AND M. R. KUNDU
Astronomy Program, University of Maryland, College Park
Received 1977 September 19; accepted 1977 November 21

ABSTRACT

Nine 6 cm solar bursts were observed with the Westerbork Synthesis Radio Telescope on 1974 May 8–10. The bursts were of weak to moderate intensity. One-dimensional fan-beam scans with resolution of up to 6″ were obtained every 30 s. The spatial structure and the time evolution of the bursts are discussed. The bursts occurred near the weak components of associated 6 cm active regions and quite often near the neutral line of the magnetic field. At the time of maximum intensity the estimated brightness temperatures ranged from 10^6 to 2×10^7 K and their angular sizes ranged from 7″ to 23″. An expansion of the burst core after maximum intensity was observed in most cases. We also observed a drift in the position of the burst core. Around the time of maximum intensity the bursts were circularly polarized in the sense of the extraordinary mode. The sense of circular polarization was the same over the entire extent of the burst source; this suggests that if the burst is associated with loop structures, the emission must be associated with one leg of the loop. No polarization was detected in the postburst phase. This implies that the nonthermal electrons responsible for gyrosynchrotron radiation during the impulsive phase become thermalized in the postburst phase; from the absence of polarization one can deduce an upper limit of 20–50 gauss for the magnetic field in the burst region.

Subject headings: polarization — Sun: flares — Sun: magnetic fields — Sun: radio radiation

I. INTRODUCTION

The presence of small-scale structure in centimeter wavelength burst sources was established by Kundu (1959), who obtained estimates of burst sizes between 1′ and 3′.5 with a two-element interferometer. Since that time there have been a number of observations with fan beam interferometers, primarily from Toyokawa (e.g., Enomé, Kakinuma, and Tanaka 1969) with spatial resolution as good as 24″ and more recently from Stanford (e.g., Felli, Pallavicini, and Tofani 1975) with 16″ resolution, which have revealed smaller scale structures and more complexity in the burst regions. Significantly better resolution of 3″–9″ has been achieved with the NRAO interferometer; observations with such spatial resolution have revealed structures of only a few arc seconds (see, e.g., Hobbs *et al.* 1973; Kundu, Becker, and Velusamy 1974; Alissandrakis and Kundu 1975). At the same time X-ray observations, particularly from *Skylab*, with resolution better than 2″ (e.g., Kahler, Krieger, and Vaiana 1975; Vorpahl *et al.* 1975) have given new information about the flare phenomenon; these observations are of particular relevance to the centimeter-wavelength observations due to the close association of X-ray and centimeter-wavelength burst sources (Kundu 1961; Kundu, Alissandrakis, and Kahler 1976; Pallavicini and Vaiana 1976).

The NRAO interferometer, with only three baselines, cannot give any information about complex structures in burst sources and is relatively insensitive to large-scale structures (Alissandrakis and Kundu 1975). The Westerbork Synthesis Radio Telescope (WSRT) does not have these disadvantages while at the same time it has comparable angular resolution. We have used this telescope on 1974 May 8–10 for two-dimensional synthesis of solar active regions (Kundu and Alissandrakis 1975; Alissandrakis 1977; Kundu *et al.* 1977).

In the course of our observations with the WSRT we observed several bursts at 6 cm. Since the bursts are rapidly varying phenomena, it is not possible to produce a two-dimensional image from observations with a one-dimensional interferometer array; however, we have enough baselines (20 in total) to get one-dimensional intensity scans (fan beam scans) and therefore study the structure, position, and evolution of the bursts. The integration time of 30 s limits our ability to detect variations on a shorter time scale; it also decreases (by the averaging effect) the observed intensity of the peaks of explosive events, which can be of much shorter duration. In this paper, we present the results of 6 cm burst observations as obtained with a one-dimensional resolution of up to 6″.

II. OBSERVING PROCEDURE

The WSRT consists of twelve 25 m paraboloids on an E–W baseline (Högbom and Brouw 1974); of these, two, which we will refer to as A and B are movable: A is closest to the east of the fixed telescopes, and can be placed anywhere on a rail track 300 m long. Each fixed telescope is combined with each movable one, resulting in 20 interferometer pairs. For our observations, the minimum spacing was 90 m, the maximum 1458 m, the separation between successive baselines 72 m. The minimum spacing was chosen in order to avoid significant shadowing of the dishes at

low elevations, although a smaller minimum spacing would be desirable for better detection of extended sources. The synthesized two-dimensional beamwidth at 6 cm for a source at $\delta \approx 17°$ (the Sun's declination at the time of observations) is 6.″3 (E–W) × 21.″5 (N–S), and the primary beamwidth is ~10′. The time constant of the system is ~20 s; each correlator channel is sampled every 10 s, and the average of three samples is recorded on tape; thus the effective integration time is 30 s. For polarization measurements each WSRT telescope is equipped with a pair of perpendicular dipoles. We have used the standard observing mode in which the dipoles of the movable dishes form a 45° angle with respect to those of the fixed telescopes. The four Stokes parameters were obtained by linear combinations of the correlated outputs of all dipole combinations (Weiler 1973).

The use of a sidereal instrument for solar observations gives rise to certain problems caused by the very high radio intensity of the Sun and by the changing coordinates of a solar region. These problems were successfully dealt with and have been discussed in detail in the works of Alissandrakis (1977) and Kundu *et al.* (1977). For burst observations there is also a danger of saturation of the correlators, since the bursts have brightness temperatures of millions of degrees above the active region background and the correlators were adjusted for best detection of active regions. This is more serious for the shortest baseline which picks up the largest correlated flux. A saturation even in a single channel would produce significant distortions both in the measured intensity and the position of the burst source; furthermore, if such a saturation lasts for a shorter time than the integration time, it may not be detectable by inspection of the correlator output. For this reason we checked for saturation effects in the brightest burst observed by processing the data twice: one using all baselines and the second time omitting the data from the shortest baselines. The fact that we obtained nearly identical results indicates that the saturation, if any, is negligible.

III. ONE-DIMENSIONAL SYNTHESIS WITH THE WSRT

A linear array, such as the NRAO or the WSRT instruments, cannot give two-dimensional maps of the rapidly varying burst sources. In the past, with the NRAO interferometer (Kundu, Velusamy, and Becker 1974; Alissandrakis and Kundu 1975), we have used simple source shapes to model the visibility function and get some information about the burst source structure. With the WSRT, however, it is possible to get one-dimensional (fan beam) scans every 30 s and thus study the structure and evolution of burst sources much better than with the NRAO interferometer. The detailed procedure of using the WSRT as a fan beam instrument is given in the Appendix.

The fan beam gives resolution along the direction of the projected baseline on the plane of the sky. This direction changes during the 12 hour observing period, so that at zero hour angle we can resolve structures in the E–W direction and at hour angles of ±90° we can resolve structures along the N–S direction. At the same time the length of the projected baseline changes and consequently the width of the fan beam changes during the 12 hour period. The position angle of the direction of resolution and the relative width of the fan beam are shown in Figure 11, as functions of the hour angle of the source.

Although the fan beam provides resolution along one direction, if the direction of baseline changes considerably during the lifetime of a structure it is possible to calculate its position precisely on the plane of the sky. However, if the structure is short lived, we can only calculate the locus of possible positions of the structure; this locus is a straight line perpendicular to the direction of resolution.

The one-dimensional beam pattern at zero hour angle is shown in Figure 12, and it has some similarities with the two-dimensional beam. The untapered beamwidth is 4.″9 which is smaller than the width of the two-dimensional beam but at the same time it has more pronounced ripple. For the present work a Gaussian tapering function was used with a value of 0.25 at the maximum baseline. This reduced considerably the ripple of the beam pattern while at the same time it increased the beamwidth to 6″ (Fig. 12). At the position of the grating rings of the two-dimensional beam, the fan beam has prominent grating lobes. The whole beam pattern repeats itself after a distance of 11.′4 (~⅓ of the diameter of the solar disk), and this introduces some ambiguity in the position of a source. However, since the primary beamwidth is ~10′ and the active regions were well separated, there was no problem in associating a burst with a particular active region.

We should note here that if telescope A had been placed at a distance of 72 m from telescope 9, the repetition distance of the beam pattern would have been only 2.′9 and this would have made the ambiguity in the true position of a burst source much worse.

As in the two-dimensional synthesis, the fan beam is not sensitive to large sources. The relative sensitivity, defined here as the ratio of the observed to the true intensity of a Gaussian shaped source, is shown in Figure 13 and is less than 50% for sources larger than 62″ at zero hour angle.

A summary of the parameters of the one-dimensional synthesis as a function of the hour angle of the source, h, is given in Table 1.

IV. DATA PROCESSING

The burst observations were calibrated and corrected for solar motion together with the active region data as described by Alissandrakis (1977) and by Kundu *et al.* (1977). Subsequently the burst data were treated separately by using a set of programs developed at the University of Maryland for a Univac 1108 computer. A one-dimensional Fourier transform was performed using all data of each 30 s interval, and fan beam scans were obtained of all Stokes parameters.

The problem of removing the grating lobes is more

TABLE 1

ONE-DIMENSIONAL SYNTHESIS WITH THE WSRT

Synthesized beam FWHM (untapered).....	$4'.9 \times F(h)$; $F(h) = (\cos^2 h + \sin^2 h \sin^2 \delta)^{-1/2}$
Grating lobe distance.....	$2'.9 \times F(h)$, $5'.7 \times F(h)$, etc.
Pattern repetition distance.....	$11'.4 \times F(h)$
Sensitivity bandwidth to Gaussian sources.....	$2'' \times F(h)$ to $62'' \times F(h)$

severe here than in the two-dimensional case, since their intensity is much stronger in this case; it is extremely difficult when a burst occurs near a grating lobe of an active region, as in the case of some of our bursts. After several methods were tested (e.g., direct cleaning, least square fit of the visibility function to Gaussian sources, subtraction of the visibility just before the start of the burst, subtraction of constant sources), the following method seemed to be the best: (*a*) Subtract the response of constant sources. (*b*) Do the one-dimensional Fourier transform. (*c*) Clean the Fourier transform using a method similar to the one used in the two-dimensional case. (*d*) Add back the subtracted sources. This method enabled us to obtain "clean" scans with residual intensity of grating lobes of a few percent.

V. RESULTS

The results of observing 6 cm bursts with the WSRT as a fan beam instrument are presented in this section in the form of contour diagrams giving the one-dimensional intensity of the Stokes parameters I (total intensity) and V (circular polarization) as a function of position and time in Figures 1–5; the position of the preexisting constant source is marked by an arrow labeled with a letter identifying some component in that source (see Figs. 4 and 7 of Kundu *et al.* 1977). The figures also give the total intensity and circular polarization flux as a function of time. No linear polarization was detected.

A summary of the burst data is given in Table 2. The bursts are identified by two numbers, the first giving the day of 1974 May on which the burst was observed and the second being its sequence number. In Table 2 also are indicated regions 2, 3 (see Kundu *et al.* 1977) in which the bursts occurred. In addition to relevant instrumental parameters, the table provides values of flux, one-dimensional size, as well as estimates of burst brightness temperature at the time of each burst peak. The data given in Table 2 were derived from scans from which all constant sources had been subtracted; it is clear that this subtraction will result in an underestimation of the brightness temperature if a burst occurred at the same place as a preexisting strong source and if the burst were optically thick. This might particularly affect bursts 8-2, 8-3, 9-1, and 9-3 which have *projected* one-dimensional positions very close to the *projected*

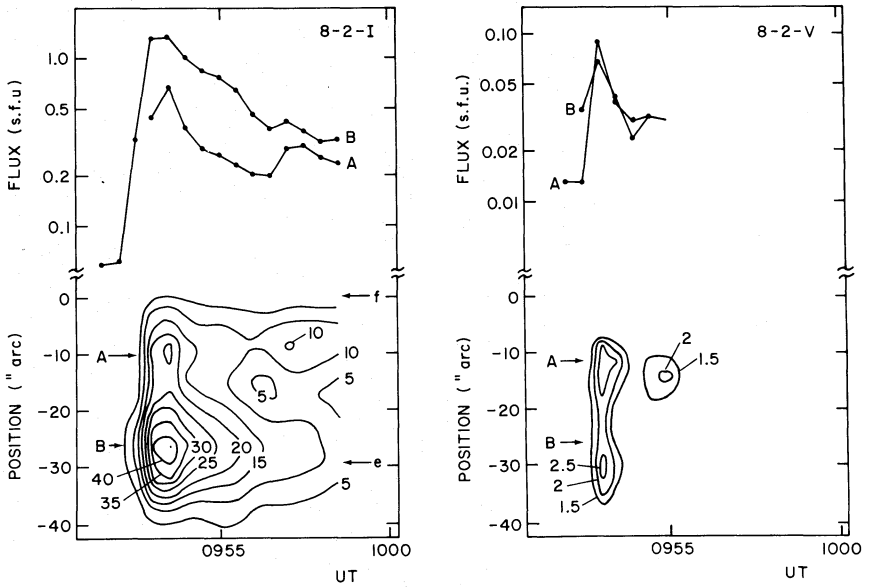

FIG. 1.—Total intensity (I) and circular polarization (V) data of the burst 8-2. The upper part of the figure shows the flux in solar flux units as a function of time, while the lower part shows the one-dimensional brightness temperature as a function of position and time. Contour labels are in units of 10^6 K arcsec. Negative polarization values (*dashed contour lines*) correspond to left-hand circular polarization.

The position of constant sources near each burst is shown by arrows on the I contour maps, labeled with a lowercase letter identifying some component of the synthesized map (see text and Kundu *et al.* 1977). All constant sources have been subtracted from this particular figure for better presentation of the burst data. In Figs. 2–8 the contours of constant sources are parallel to the time axis.

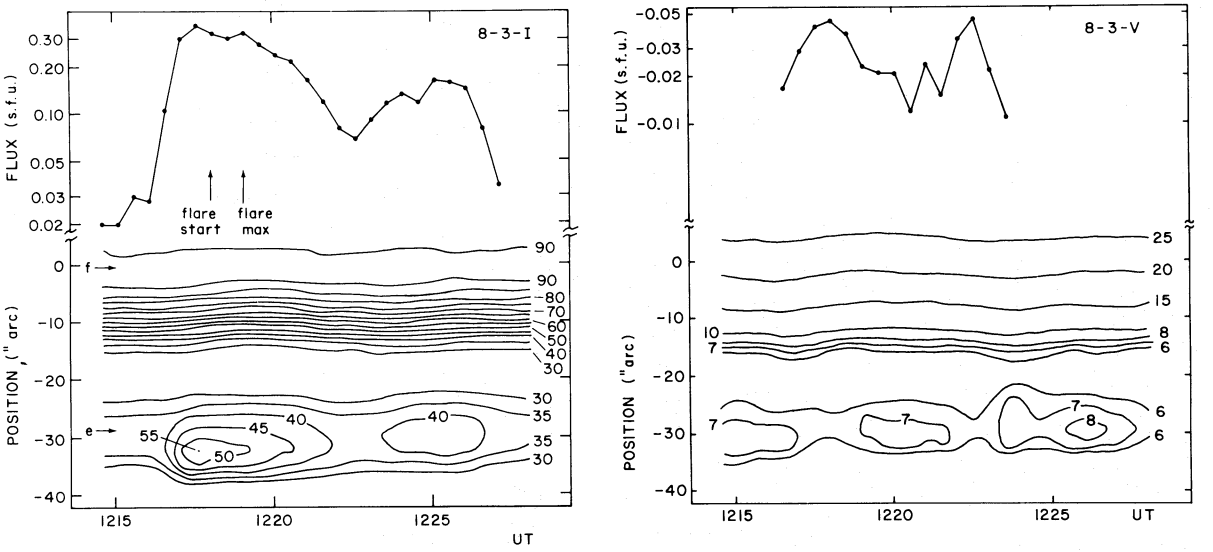

FIG. 2.—Same as Fig. 1 for burst 8-3

positions of the preexisting constant sources; however, it is not possible to determine from one-dimensional observations whether a burst occurred right on the top of another source.

From our observations we can only give the locus of possible positions of the burst, which is a straight line as discussed earlier. The position lines of the brightest peak of each burst have been drawn on the corresponding radio maps of active regions (See Figs. 4 and 7 of Kundu *et al.* 1977). The distance of each peak from the center of the field of view, measured along the direction of the projected baseline, is also given in Table 2; this will serve mainly for comparison of the positions of the *I* and *V* peaks or of different peaks of the same burst. In the course of some bursts we observed a shift in the position of the peak emission. Since the orientation of the projected baseline changes with time, such a shift is expected to occur in stationary sources that are not located at the center of the field of view; alternatively, the effect could be due to a real displacement of the burst source. Assuming that a source is stationary we can calculate its x and y coordinates from the one-dimensional position and its rate of change. Such calculations gave positions that were too far outside the field of view and therefore we conclude that the observed shifts were mainly due

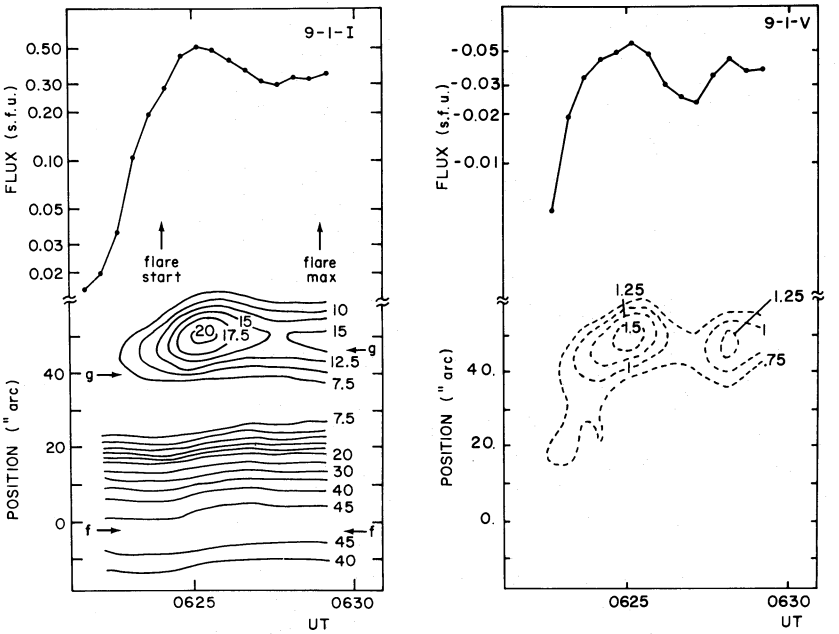

FIG. 3.—Same as Fig. 1 for burst 9-1

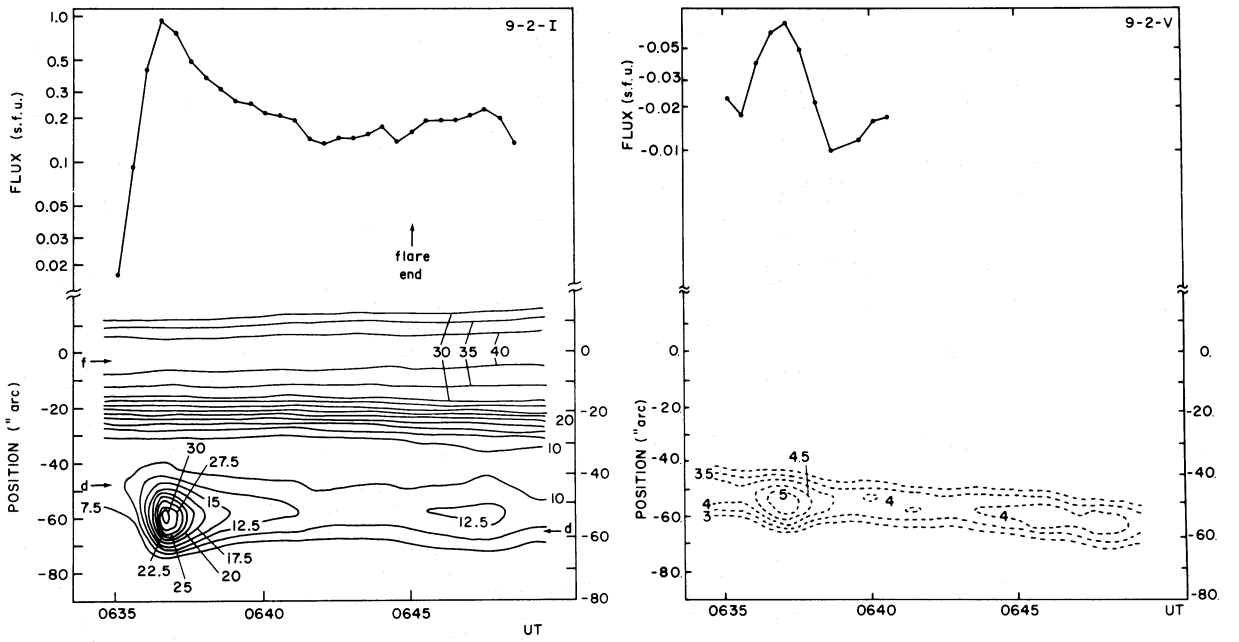

FIG. 4.—Same as Fig. 1 for burst 9-2

to real displacements of the sources. In some cases we also observed a change in the direction of the shift, which could not be interpreted as a baseline effect.

The source flux, source position, and the observed full width at half-maximum (FWHM) were derived from a fit of the one-dimensional intensity scan to a model Gaussian source; the fit was quite good, with typical errors of a few percent for flux and FWHM and less than 1″ for the position. The true FWHM was determined after taking into account the instrumental angular resolution. No calculation was attempted for cases where the observed FWHM was nearly equal to the angular resolution. Finally, the estimate of the brightness temperature was obtained from the flux and the corrected FWHM under the assumption that the burst source is circularly symmetric; since it is well known that chromospheric flares often show a ribbon-like structure, this assumption may not be valid for all cases. Temperatures and fluxes have been corrected for primary beam attenuation, both in Table 2 and in the figures.

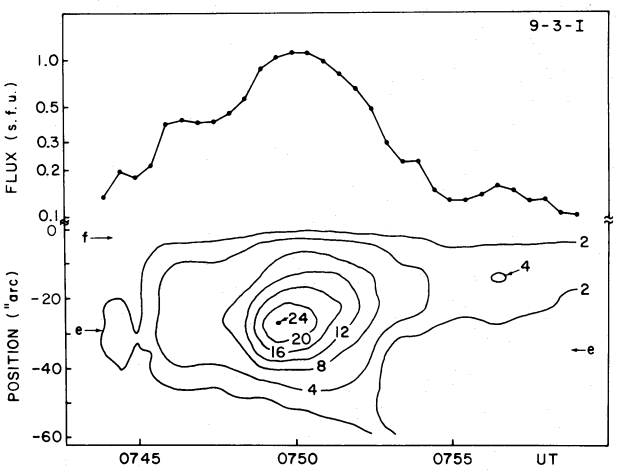

FIG. 5.—Same as Fig. 1 for burst 9-3. All constant sources have been subtracted from this figure.

VI. DISCUSSION OF INDIVIDUAL BURSTS

Five bursts were observed in the eastern part of the McMath region 12906 (region 2). Three of them occurred in the vicinity of component *e* (Fig. 4 of Kundu *et al.* 1977), while the other two were apparently associated with components *d* and *g* of the 6 cm active region. All five bursts were weak in intensity (only burst 9-1 was observed by total Sun patrol instruments at centimeter wavelengths), and in circular polarization. Plots of the intensity of these bursts are shown in Figures 1 to 5.

Burst 8-2 (Fig. 1) was an event of impulsive type with the usual fast rise to maximum and subsequent slow decay. A very interesting feature of this event is that it consisted of two spatially distinct bright regions, A and B, with region B lying very close to component *e* while A was located close to the main peak of the 6 cm emission of region 2 (component *f*). Both regions reached maximum intensity at the same time, but region B had a faster rise; region A has a weak secondary maximum while B has a smoother postburst decay. Both regions were right circularly polarized for a short time around peak intensity.

Another burst occurred near the same location two hours later (burst 8-3, Fig. 2) and it was associated with an "unconfirmed" Hα flare of importance −F. This burst had only one spatial component with a fast rise to maximum intensity, a slow subsequent decay,

TABLE 2

SOLAR BURSTS OBSERVED WITH THE WSRT AT 6 cm, 1974 MAY 8–10

BURST	REGION	θ* (deg.)	RESOLUTION (arcsec)	TOTAL INTENSITY (I) UT	Position (arcsec)	FWHM† (arcsec)	T_b‡ (10^6 K)	Flux (s.f.u.§)	CIRCULAR POLARIZATION (V) UT	Position (arcsec)	FWHM† (arcsec)	T_b‡ (10^6 K)	Flux (s.f.u.§)
8-1.....	3	−79	7.1	09 12.7	...	...	...	...	09 12.7	...	...	...	...
8-2.....	2	−83	6.5	09 53.5	−27.1	14.1	3.2	1.31	09 53.0	−30.2	16.0	0.2	0.09
				09 53.5	−9.6	12.7	2.0	0.67	09 53.0	−13.6	10.9	0.3	0.07
				09 57.0	−8.6	‖	‖	0.29	...	...	...	...	...
8-3.....	2	−94	6.1	12 17.6	−33.9	7.1	3.5	0.36	12 17.6	−34.0	‖	‖	−0.04
				12 25.5	−31.9	8.9	1.16	0.1	...	...	...	...	...
9-1.....	2	−40	16.0	06 25.1	51.0	‖	‖	0.51	06 25.1	53.1	‖	‖	−0.06
				06 28.1	49.5	‖	‖	0.33	06 28.1	51.1	‖	‖	−0.04
9-2.....	2	−46	14.8	06 36.5	−58.8	10.0	4.6	0.93	06 37.0	−58.6	‖	‖	−0.08
				06 47.5	−55.3	15.5	0.5	0.22	...	...	...	...	...
9-3.....	2	−67	9.6	07 49.4	−25.0	22.5	1.0	1.06	...	...	...	...	...
9-4.....	3	−86	6.1	10 39.9	39.9	11.7	8.5	2.37	10 39.4	36.8	9.7	2.9	0.55
				10 42.4	37.4	14.0	6.5	2.58	10 42.4	37.2	8.9	2.1	0.33
				10 44.4	48.3	12.9	3.3	1.11	...	...	...	...	...
				10 46.4	32.8	14.7	11.3	4.97	10 46.4	33.1	11.3	1.0	0.25
9-5.....	3	−104	7.6	14 11.4	22.6	12.1	3.2	0.96	14 10.9	21.7	11.4	1.4	0.34
				14 15.4	22.5	13.8	2.3	0.86	14 15.4	22.7	11.1	0.5	0.13
9-6.....	3	−135	15.0	16 24.0	−11.6	17.4	19.2	12.00	16 24.0	−9.8	14.2	2.6	1.06

* Position angle of projected baseline measured counterclockwise from celestial north.

† Corrected for instrumental resolution.

‡ Calculated under the assumption of a circularly symmetric Gaussian source.

§ 1 solar flux unit (s.f.u.)-10^{-22} W m^{-2} Hz^{-1}.

‖ Unresolved source.

and a weaker secondary maximum 7 minutes later; the first maximum is weakly circularly polarized in the left-hand sense, while no polarized emission could be associated with the second maximum, although there was some increase in polarization flux one minute before the second maximum. The burst polarization shows up in Figure 2 as a decrease in the right-hand circular polarization of a preexisting source.

The first burst observed in region 2 on May 9 occurred in the vicinity of component *g* (burst 9-1, Fig. 3). This particular burst was also observed by total Sun patrol instruments at 8 cm (*Solar Geophysical Data* 1974). Both in total intensity and in circular polarization it showed up as a small feature, almost unresolvable, so it is not possible to give estimates of its true size and brightness temperature. Its time evolution showed a rather slow rise to maximum followed by a slow decay and a secondary maximum, barely visible in the total intensity but quite prominent in circular polarization. A gradual shift of the burst position to the west occurred around the first maximum with a projected speed of ~ 30 km s^{-1}. One minute after maximum the motion reversed and the burst was moving to the east at about 10 km s^{-1}.

Burst 9-2 started 10 minutes later, but at a different location (near component *d* of the active region). Its evolution is shown in Figure 4; it had a quick rise to maximum and a slow decay. A weak second peak appeared 12 minutes later, but it is not clear whether this is part of the same event or is a separate phenomenon. The burst maximum was weakly circularly polarized in the left-hand sense. A weak Hα flare (importance −F) was reported and may be associated with the burst, but there was no good correspondence between the times of maximum of the two events (see Tables 2, 3).

The last event observed on May 9 in region 2 was burst 9-3 (Fig. 5) which occurred in the vicinity of component *e* of the active region. It was of type "gradual rise and fall," fairly large in size ($\sim 23''$), without any detectable circular polarization. The main peak was followed by a very weak secondary maximum 7 minutes later. After maximum there was an appreciable drift of the burst source toward the component *f* of the active region with an apparent speed of 10 km s^{-1}.

A total of four bursts were observed in region 3 (western part of McMath 12906), one on May 8 and three on May 9; these include the two strongest bursts observed with the WSRT. The three bursts on May 9 were all recorded by patrol instruments and were associated with Hα flares.

Burst 8-1 was a weak event that took place near a small 6 cm component in the east of region 3 (Fig. 7 of Kundu *et al.* 1977) on May 8. Unfortunately, it was very close to a grating lobe of region 2; and this, combined with its low intensity, did not allow us to get an estimate of its size and temperature. We can say that it was a short event with some circular polarization.

Burst 9-4 (Fig. 6) was the most spectacular of all bursts observed; it lasted for more than 30 minutes, had four distinct peaks at different locations, and was associated with a 1B Hα flare. The flare was described in *Solar Geophysical Data* as having several eruptive centers, which were probably associated with the 6 cm peaks; in this respect it was similar to an event observed by Alissandrakis and Kundu (1975) at 3.7 and 11.1 cm with the NRAO interferometer. Patrol observations reported two maxima at 6 cm coinciding with our maxima at 10 39.0 and 10 46.4 UT. The burst was located in the vicinity of component *b* of region 3 (Fig. 7 of Kundu *et al.* 1977), and the maximum distance between the position of the peaks along the E–W direction was about 15″. The peak at 10 39.9 UT showed the strongest circular polarization ($\sim 40\%$ right handed), while the peak at 10 46.4 UT, which was the strongest in total intensity, was only 12% polarized. The weak peak at 10 44.4 UT was not polarized at all.

The emission peaks in total intensity were superposed on top of a broad background which is asymmetric, being broader in the direction away from the active region. This background emission was absent in the circular polarization image of the source which was smaller in size. In the decay phase of the burst, shortly after the peak at 10 46.4 UT, there was no detectable circular polarization.

TABLE 3

Hα FLARES BETWEEN 0550 AND 1730 UT, 1974 MAY 8–10, REPORTED IN *Solar Geophysical Data*

Date (1974 May)	Flare Number	UT Start	UT Maximum	UT End	Location	Region	Area (arcsec^2)	Importance	Associated Burst
8.....	60 147	1218	1219	1230	S13 W08	2	135	−F	8-3
	60 148	1225	1227	1240	S04 W38	4	88	−F	*
	60 150	1546	1548	1554	S05 W40	4	110	−−F	*
9.....	60 157	0624	0629	0645	S09 W16	2	273	−−F	9-2?
	60 158	0825	0828	0843	S05 W36	3	149	−−N	*
	60 159	1036	1047	1101	S05 W38	3	638	1B	9-4
	60 160	1301	1304	1325	S04 W37	3	566	−−F	†
	60 161	1409	1413	1427	S05 W40	3	215	−N	9-5
	60 162	1619	1628	1653	S05 W40	3	569	1N	9-6
10.....	60 166	0809	0811	0817	S02 W74	4	118	−−F	†
	60 167	1428	1430	1441	S05 W52	3	99	−−F	*

* Occurred during a gap in our 6 cm observations.

† Occurred at a time when the sidelobes from Region 2 were crossing the flare region.

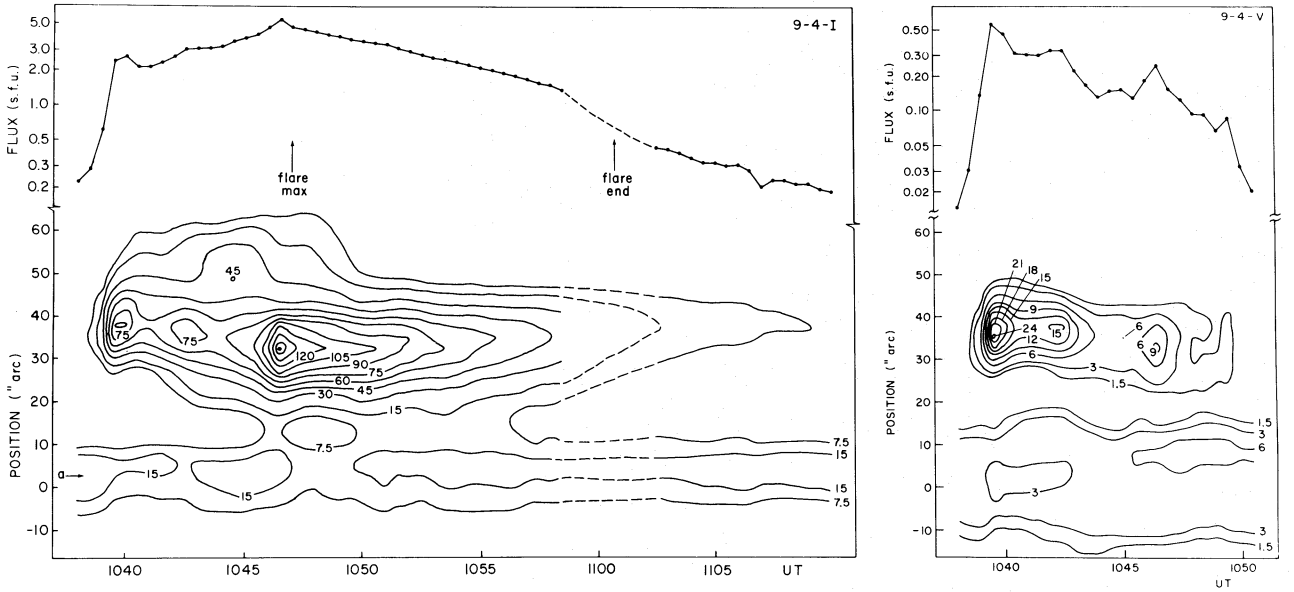

FIG. 6.—Same as Fig. 1 for burst 9-4. The dashed lines indicate a gap in our observations for updating the antenna pointing.

As mentioned above, the different peaks of the burst 9-4 did not occur at the same place. If we ignore the peak at 10 44.4 UT which was located outside most of the burst source, the brightest point of the source drifted to the east with an apparent speed of ~18 km s^{-1} between 10 39.9 and 10 46.4 UT. The position of the brightest point remained stationary for about 4 minutes after the peak at 10 46.4 UT and then started moving to the west at a much lower projected speed of ~5 km s^{-1}, so that near the end of the event at 1105 UT it returned to the same position as that of the first peak.

At 1409 UT another flare of importance −N occurred in almost the same location and gave rise to burst 9-5 (Fig. 7). This event had a simpler spatial structure than the previous burst, with two peaks at nearly the same location; the first peak had the strongest circular polarization (~23% right handed). The two events, 9-4 and 9-5, can be considered as "homologous" bursts since they occurred at the same place and had a similar evolution.

The most intense burst was the impulsive event 9-6 (Fig. 8) with a rise in brightness temperature to about 20 million degrees (Table 2) in less than 2 minutes. The decay phase of this event lasted about 20 minutes. Unfortunately we missed about 3.5 minutes of data during this period because of a prescheduled update of the telescope pointing, with the result that we do

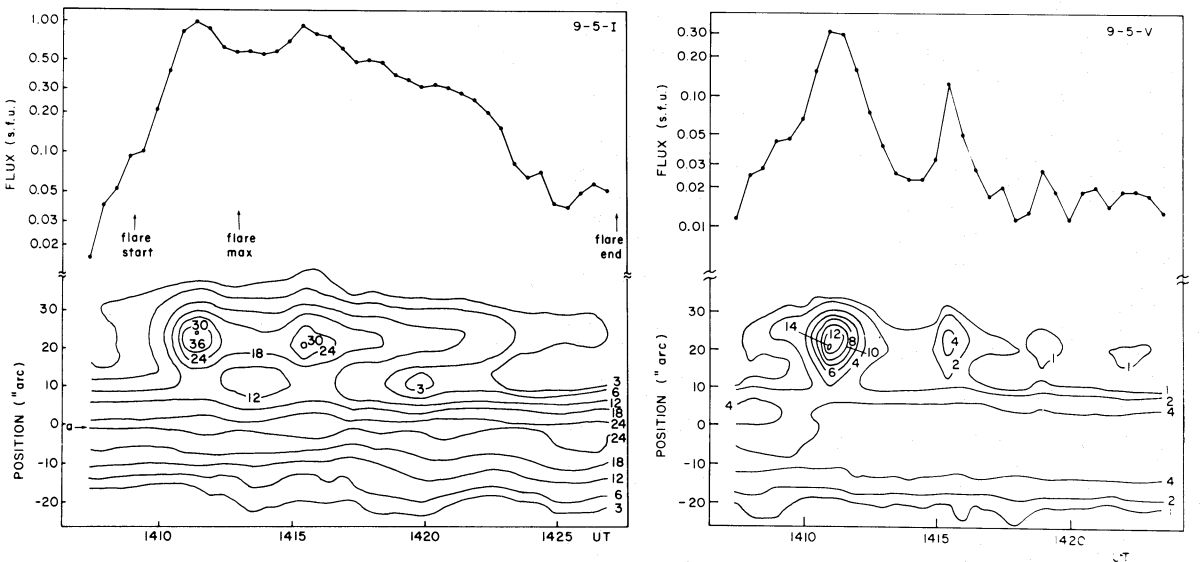

FIG. 7.—Same as Fig. 1 for burst 9-5

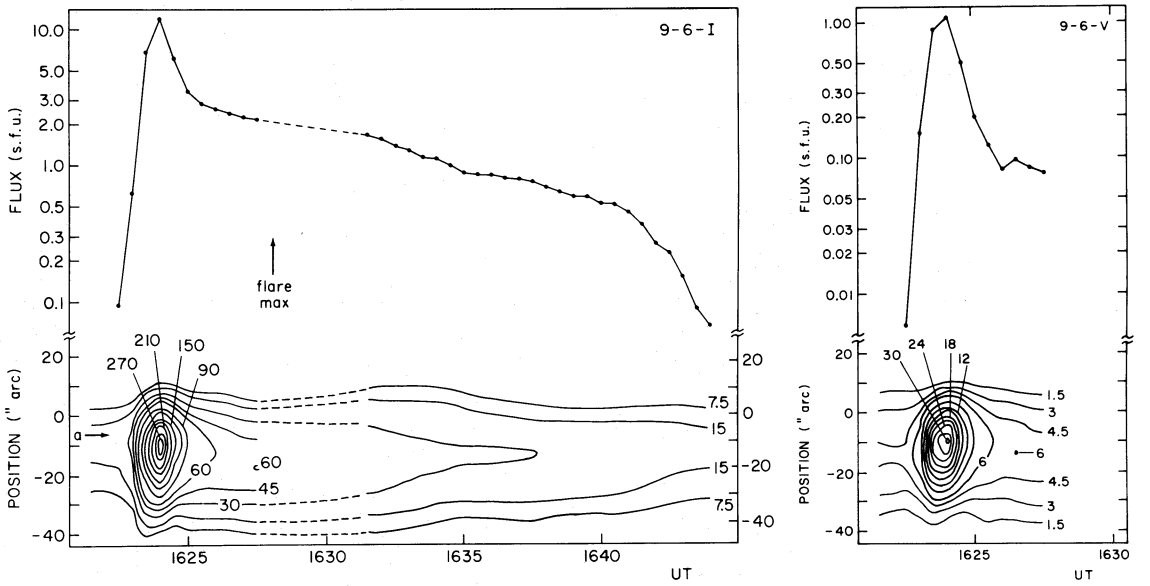

FIG. 8.—Same as Fig. 1 for burst 9-6. The dashed lines indicate a gap in our observations.

not know if there were any secondary peaks; there is, however, evidence of increasing brightness just before the gap in our observations. The polarization of the burst was rather low (13% right handed), and it was observed only for 4.5 minutes around the maximum, the rest of the burst being unpolarized. A movement of the brightest point of the burst source was observed for 3 minutes after maximum at a speed of ~ 35 km s^{-1}; there was little motion during the rest of the decay phase.

VII. CORRELATION WITH Hα FLARES

Precise knowledge of the nature of centimeter bursts is essential for understanding the flare phenomenon as a whole. Consequently, it is interesting to compare the present observations with Hα flares and radio bursts at longer wavelengths. Unfortunately, no X-ray observations were available for this period.

A list of all Hα flares from regions inside our field of view is given in Table 3. Four bursts were definitely associated with Hα flares, while there were six small flares for which we observed no associated burst. One of them, 60150, did produce a centimeter-wavelength burst observed by patrol instruments. However, it occurred during a gap in our observations for a pointing update. Three more flares (60148, 60158, 60167) occurred during observation gaps. Two flares (60160 and 60166) occurred at a time when sidelobes from region 2 were crossing the flare region, making the detection of any weak burst impossible.

For three bursts no associated Hα flares were reported, although there were no gaps in the flare patrol at the time of their occurrence. Since all three were weak events (flux of ~ 1 sfu[1] or less), one possibility is that they were associated with low-intensity Hα brightenings that did not qualify as flares; on the other hand, they may have been associated with other Hα phenomena (e.g., activation of filaments). However, examination of Hα patrol films from Big Bear Observatory for a limited time during our observations did not reveal any special chromospheric event associated with these bursts.

The times of start, maximum, and end of the Hα flares are shown in Figures 2, 3, 4, 6, 7, and 8. There is some ambiguity as to whether flare 60157 is associated with burst 9-1 or 9-2, and therefore it was excluded from the following discussion. It is important to note that in all cases the first peak of the 6 cm emission occurred before the flare maximum, probably during the flash phase of the flare. In the case of intense bursts 9-4 and 9-6 the burst started after the flare start, while in two other cases, 8-3 and 9-5, the burst started earlier. In many cases the flare lasted longer than the burst, but we must keep in mind the uncertainties involved in deciding exactly when a flare or a burst ends.

The accuracy of flare positions given in *Solar Geophysical Data* is only of the order of 1° in heliocentric coordinates, which amounts to about 15″. A comparison of these positions with those of our 6 cm bursts showed a tendency for the bursts to lie to the west of the flares, indicating that the bursts occurred higher in the solar atmosphere. On this basis a height of 20×10^3 km was obtained for the burst sources with an uncertainty of about a factor of 2. Finally, a comparison of the flare area and the burst size showed a positive correlation; that is, the burst size was larger when the Hα flare size was larger. We cannot make a more exact comparison since we do not know the exact shape of the bursts.

Three bursts (9-4, 9-5, and 9-6) were observed by patrol instruments over a wide range of wavelengths,

[1] 1 solar flux unit (sfu) = 10^{-22} W m^{-2} Hz^{-1}.

extending to meter waves. This is a well-known phenomenon which implies that centimeter emission at lower heights in the solar atmosphere is sometimes associated with instabilities higher up in the corona resulting in radio emission at longer meter and decameter wavelengths. In the absence of comparable spatial resolution at both ends of the spectrum (cm and m wavelengths) it is impossible to draw any further conclusions from this association.

VIII. DISCUSSION

With the exception of bursts 9-1 and 9-3, all others are of impulsive nature with a fast rise and a slow postburst decay, sometimes with superposed secondary peaks; bursts 9-3 and possibly 9-1 are closer to the "gradual rise and fall" type (Kundu 1965). With the exception of 9-4 and 9-6, the bursts are very weak events with maximum flux of the order of 1 sfu, which is close to the lower limit that can be detected by patrol instruments.

Previous high-resolution burst observations (Kundu, Becker, and Velusamy 1974; Alissandrakis and Kundu 1975) showed a discrepancy between the burst flux obtained by patrol instruments and that derived from fitting the fringe visibility to model sources, the former being considerably larger than the latter; this was interpreted as resulting from the reduced sensitivity of the interferometer to large scale components of the burst emission. For the present observations we can make this type of comparison for bursts 9-4 and 9-6, which are the only ones for which 6 cm flux densities have been reported in *Solar Geophysical Data*, from both the Athens and Sagamore Hill observatories. Our observed values of the maximum flux for bursts 9-4 (last peak) and 9-6 are in good agreement with the flux reported by Athens; it is, however, lower by a factor of 2 than the flux reported by Sagamore Hill for 9-4 (first peak) and 9-6. It is not clear what caused the discrepancy in the flux values given by the two observatories, mainly because they gave consistent flux values at 6 cm for most other bursts in 1974 May. In any case, there is better agreement between the flux values measured by the present WSRT interferometric observations and those measured by single dishes than in the case of our previous NRAO observations. We attribute this better agreement to the increased sensitivity of the WSRT to large scale structures as discussed in an earlier section.

The sizes of our burst sources range between 7″ and 23″, in fair agreement with the NRAO interferometer observations (Kundu, Velusamy, and Becker 1974; Hobbs *et al.* 1973; Alissandrakis and Kundu 1975); they are smaller than the value of 1′ obtained by Kundu (1959) for weak bursts at 3 cm with a lower resolution interferometer and the value of 30″ reported by Enomé, Kakinuma, and Tanaka (1969). On the other hand, the 6 cm burst sizes measured with the WSRT are in good agreement with those obtained for X-ray bursts (Kahler *et al.* 1975; Vorpahl *et al.* 1975). The "gradual rise and fall" burst 9-3 had the largest size ($\sim 23''$) and the lowest brightness temperature ($\sim 10^6$ K).

From previous observations by Kundu (1959) we know that the size of impulsive bursts increases in the postmaximum phase, an evidence of expansion of the burst source. An example of such behavior is shown in Figure 9, where the FWHM of burst 9-4 is plotted as a function of time; the FWHM was calculated from a least squares fit of the core of the burst to a Gaussian model source excluding the weak peak at 10 44.4 UT. The arrows mark the times of the maxima at 10 39.9, 10 42.4, and 10 46.4 UT. As the intensity increases, the burst source contracts, reaching a minimum size near the first intensity maximum; this is followed by an expansion at an apparent velocity of ~ 30 km s^{-1}. The expansion stops 2 minutes before the second maximum and is followed by a slight contraction. After the second maximum there is again an expansion at ~ 60 km s^{-1}, followed by a contraction as the burst reaches its last maximum. There is a slow expansion after the last maximum followed by a long period during which the burst size remained constant. The size of the polarized emission had a similar behavior (Fig. 9), but the changes in size are less prominent. Of the other events, burst 9-6 showed a vigorous core expansion at ~ 70 km s^{-1} while the weaker bursts expanded rather slowly (< 10 km s^{-1}).

In the course of four bursts we observed a gradual displacement of the brightest point of the burst source. Such a displacement does not necessarily imply that the burst material was moving, since it could be the result of the consecutive brightening of different parts

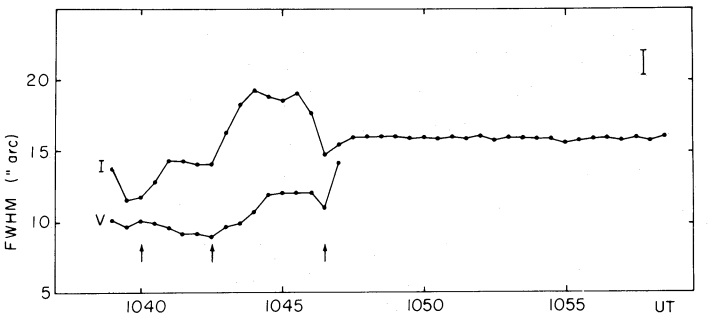

FIG. 9.—Plot of the full width at half-maximum (FWHM) of the core of burst 9-4 in total intensity (I) and circular polarization (V) as a function of time. The arrows show maxima in the I emission. The FWHM has been corrected for instrumental resolution.

of the burst region. An interesting behavior was observed in an X-ray burst by Vorpahl *et al.* (1975): during that event there was a consecutive brightening of the tops of a series of loop structures forming an arcade. It is possible that we observed a similar event; however, it is not possible to detect any loop structures from one-dimensional observations such as ours.

A comparison of burst sizes in total intensity and circular polarization showed that in the majority of cases the polarized emission originated from a more compact region than the total intensity emission. This is true throughout the evolution of the burst (cf. Fig. 9).

The optical observations have shown that flares occur in regions where the longitudinal component of the photospheric magnetic field has a complex structure, with regions of opposite polarity being adjacent. The basic configuration is that of a "neutral line" separating two regions of opposite magnetic polarity. Such configurations are obviously present in the vicinity of bursts 8-2, 8-3, and 9-3 which are located close to the line that separates the regions of opposite circular polarization in the V map of region 2 on May 8 (Fig. 4 of Kundu *et al.* 1977). For the other bursts one has to resort to magnetograms; indeed, an inspection of high-resolution magnetograms from Sacramento Peak and Meudon showed that the position lines of all bursts cross neutral lines of the magnetic field. In some cases the position lines cross more than one neutral line and consequently it is impossible to determine the association of the burst with a specific neutral line. The value of the longitudinal component of the photospheric field in the vicinity of the neutral lines was of the order of 25–100 gauss; no burst was associated with the intense sunspot field, with the possible exception of burst 9-6.

It is interesting to note that in all cases only one sense of circular polarization was observed and that the intensity and polarization peaks occurred very close to each other, their separation being significantly less than the size of the burst. This implies that either the burst was associated with only one branch of magnetic loop, or the neutral line was nearly parallel to the projected baseline so that the two opposite polarization components were not resolved. However, even in the latter case most of the radiation must have been associated with one polarity. With the exception of 8-3 and 9-1, the sense of the polarization is that of the extraordinary mode of the predominant magnetic field polarity in the vicinity of the burst. In the case of 9-1 an inversion of the sense of circular polarization higher in the corona was probably involved, since such an inversion occurred in the entire leading part of region 2 on May 9 (see Fig. 4 of Kundu *et al.* 1977).

Our observations show that at the beginning of the burst the circular polarization (V) rises faster than the total intensity (I). As a result the degree of circular polarization, $p = V/I$, reaches a maximum about 1 minute before the I maximum. However, only in two bursts did we observe a subsequent increase of the degree of polarization; in all other cases p decreased monotonically after the first intensity maximum and increased again only when there was a second peak in the burst emission. This result is in agreement with that of Kundu (1959) obtained at 3 cm with 1'.5 resolution. In bursts 9-4 and 9-5 secondary peaks were associated with secondary maxima in p. In all bursts with more than one maximum the largest values of both V and p were associated with the first peak.

Our observations showed no detectable polarization in the decay phase of the bursts, shortly after the last intensity maximum. This indicates that the circular polarization is primarily associated with the impulsive component of the burst. The absence of circular polarization in the postmaximum phase of the emission can be used for estimating an upper limit of the magnetic field. In this phase the burst emission is believed to be due to the free-free process. The degree of polarization of an optically thin source is (Kundu 1965):

$$p \approx \frac{2y}{1 + y^2},$$

where $y = f_H/f$, f is the frequency of observation, and f_H is the gyrofrequency. At 6 cm and with an observational upper limit of p of 2–5% we get an estimate of the magnetic field between 20 and 50 gauss. These values are lower than those used in the theoretical calculations of the burst emission (Takakura 1967) which are of the order of 500 gauss; however, they are comparable to the values of 25–100 gauss estimated from the magnetograms.

The impulsive part of the centimeter bursts is believed to be due to the gyrosynchrotron emission of energetic electrons. Indeed, the estimated brightness temperatures (up to 2×10^7 K; cf. Table 2) are indicative of the nonthermal origin of the impulsive components of some of the bursts. The postburst phase represents thermalization of the energetic electrons by collisions with particles in the ambient plasma and by expansion. The larger size and lack of polarization of the burst in the postburst phase strongly support this interpretation, originally proposed by Kundu (1959). Our present results show that this conclusion is valid even on scales of a few arc seconds.

IX. SUMMARY

During our observations with the WSRT we obtained good quality data on eight weak bursts originating in two active regions. Their structure and evolution were studied by using the WSRT as a fan beam instrument. The maximum flux of these bursts was in the range of 0.34–12.0 sfu; their size at the time of maximum intensity ranged between 7″ and 23″ and their peak brightness temperature between 10^6 and 2×10^7 K. Four bursts were clearly associated with Hα flares of importance −F to 1B; in all cases the burst maximum preceded the flare maximum. The bursts were located in the vicinity of weak components of the 6 cm emission and were associated with the "neutral line" of the magnetic field.

In most cases we observed an increase of the burst size after an intensity maximum, a possible indication of expansion. We also observed changes in the position of the burst source with an apparent velocity of 5–35 km s^{-1}; however, it is not clear whether this was due to a motion of the source or due to successive brightenings of different regions of the burst source.

The bursts were circularly polarized with the exception of a "gradual rise and fall" event which was unpolarized. The sense of circular polarization was the same over the entire extent of the burst source; this indicates that, even if the bursts were associated with loop structures, the emission was associated with one leg of the loop. In most cases the sense of circular polarization was that of the extraordinary mode.

The polarized emission was predominantly associated with the core of the impulsive component of the burst. The degree of circular polarization reached a maximum approximately 1 minute before the first intensity maximum while the postburst phase was unpolarized. From the lack of polarization in the postburst we estimated that the magnetic field in the burst region was 20-50 gauss, using an optically thin source model; this estimate is consistent with that derived from photospheric magnetograms.

The WSRT has proved to be a valuable instrument for the study of the fine structure of solar bursts at cm wavelengths. Since the radio bursts are in integral part of the flare phenomenon as a whole, such observations are important for the understanding of flares, particularly if they can be combined with simultaneous high-resolution X-ray observations. There is no doubt that large arrays such as the Westerbork Synthesis Radio Telescope will play a vital role in our understanding of the origin of solar flares.

We wish to thank the Program Committee of WSRT for scheduling us for solar observing with the Westerbork telescope. We also wish to thank Dr. H. van Someren Greve for his help during the initial period of data reduction. The help that we received from Dr. J. van Nieuwkoop of Utrecht and the members of WSRT technical group prior to observing is gratefully acknowledged. We also wish to thank Dr. P. Lantos for participating in the observations. We are grateful to Sacramento Peak Observatory for providing optical coverage and to the National Oceanic and Atmospheric Administration and the Meudon Observatory for valuable information about the position of solar active regions. We also wish to thank the Leiden and Westerbork observatories for their warm hospitality during our stay in the Netherlands.

This work was supported by NASA grants NGR 21-002-199 and NGL 21-002-033 and by NSF grant GA-43297. Computer time was supported in part by NASA grant NGS-398 to the Computer Science Center of the University of Maryland.

The Westerbork Radio Observatory is operated by the Netherlands Foundation for Radio Astronomy with the financial support of the Netherlands Organization for the Advancement of Pure Research (Z.W.O.).

Parts of this paper are based on the thesis of one of the authors (C. A.) in partial fulfilment of the requirements for the degree of Doctor of Philosophy at the University of Maryland.

APPENDIX

ONE-DIMENSIONAL APERTURE SYNTHESIS

In the standard observing mode the WSRT records a data point from each channel every 30 s. Since all telescopes are located along a straight line, this is equivalent to sampling of the visibility function along a straight line passing through the origin of the u-v plane (Fig. 10). By taking the one-dimensional Fourier transform of this function we obtain a one-dimensional brightness distribution:

$$I_1(r) = \int_{-\infty}^{\infty} V(\rho) \exp(-i2\pi\rho r) d\rho \,, \tag{A1}$$

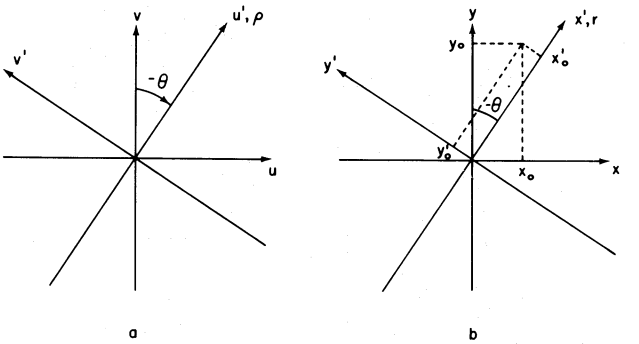

FIG. 10.—Coordinate systems for one-dimensional synthesis (fan-beam scans) (*a*) on the u-v plane and (*b*) on the sky plane

where

$$\rho^2 \equiv u^2 + v^2 = b^2(\cos^2 h + \sin^2 h \sin^2 \delta)\,, \tag{A2}$$

V is the visibility function, u and v are the projected baselines, b is the physical baseline in wavelengths, h is the hour angle, and δ is the declination of the source.

It is easy to see that I_1 is the sky intensity distribution integrated along a direction perpendicular to the projected baseline. Consider a coordinate system, u', v' (Fig. 10) with the u' axis along the sampled line of the u-v plane, and the corresponding coordinate system x', y' at the plane of the sky; then we have

$$\begin{aligned} I_1(r) &= \int_{-\infty}^{\infty} du' \exp(-i2\pi u'x') \int_{-\infty}^{\infty} V(u', v')\delta(v')dv' \\ &= \int_{-\infty}^{\infty} du' \exp(-i2\pi u'x') \int_{-\infty}^{\infty} V(u', v')\left[\int_{\infty}^{\infty} \exp(-i2\pi v'y')dy'\right]dv' \\ &= \int_{-\infty}^{\infty} dy' \int_{-\infty}^{\infty}\int_{-\infty}^{\infty} V(u', v') \exp[-i2\pi(u'x' + v'y')]du'dv' \\ &= \int_{-\infty}^{\infty} I(x', y')P(x', y')dy'\,. \end{aligned} \tag{A3}$$

Here P is the primary beam pattern and I the two-dimensional intensity distribution in the plane of the sky. In the derivation we have used the Fourier representation of the delta function.

The position angle of the positive x' axis (i.e., the direction of resolution) is given by

$$\theta = \tan^{-1}\frac{\cot h}{\sin \delta}\,. \tag{A4}$$

The synthesized FWHM is inversely proportional to the length of the projected baseline. Thus the resolution will depend on hour angle in the following manner:

$$\frac{w}{w_0} = 1/(\cos^2 h + \sin^2 h \sin^2 \delta)^{1/2} \equiv F(h)\,, \tag{A5}$$

where w_0 is the minimum FWHM of the beam (at $h = 0°$). The position angle of the direction of resolution and the relative resolution are shown in Figure 11 for $\delta = 17°$. Both change slowly near $h = 0°$ and faster at $h = +90°$.

If a source is located at a position x_0, y_0, then its location in a one-dimensional scan (Fig. 10*b*) will be

$$x_0' = -x_0 \sin\theta + y_0 \cos\theta\,; \tag{A6}$$

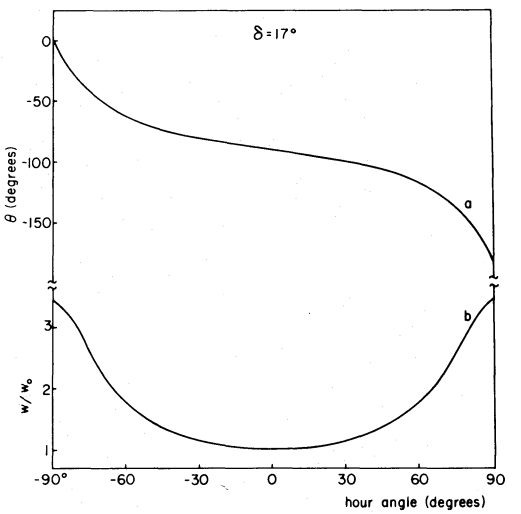

FIG. 11.—(*a*) Position angle of the projected baseline on the plane of the sky (measured from the north eastward) and (*b*) width of the synthesized beam of one-dimensional scans as a function of hour angle for a source at $\delta = 17°$.

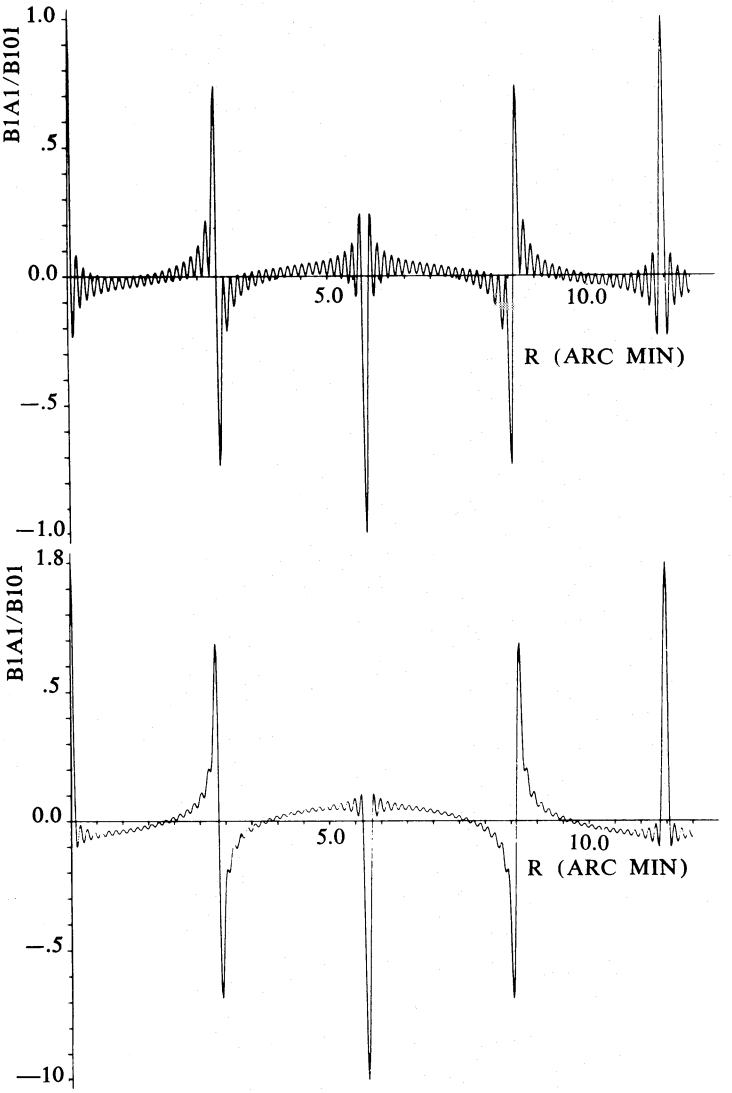

FIG. 12.—One-dimensional beam pattern at zero hour angle for WSRT with a distance of 90 m between telescopes 9 and A and 72 m between A and B. For all other angles the R scale must be multiplied by the factor given in Fig. 11*b*. A pattern (*a*) without taper and (*b*) one with a tapering function $T(b) = \exp [\ln (0.25) b^2/b_{max}^2]$ are shown.

or, in terms of h,

$$x_0' = -(x_0 \cos h + y_0 \sin h \sin \delta) F(h) . \tag{A7}$$

Conversely, if x_0' is measured, equation (A6) or (A7) defines a straight line on the plane of the sky which is the locus of all possible positions of the source.

Let us now examine the synthesized beam pattern; if ρ_j are the baselines, and $T(\rho)$ is the taper function, the beam pattern will be

$$B(r) = \int_{-\infty}^{\infty} \sum_{j=1}^{n} \delta(\rho_j) T(\rho) \exp (-i 2\pi \rho r) dr = 2 \sum_{j=1}^{n} T(\rho_j) \cos (2\pi \rho_j) . \tag{A8}$$

It is obvious from (A2) and (A8) that the beam pattern depends on the hour angle h. In the following discussion we will consider the beam at $h = 0$; the beam pattern at all other hour angles can be derived by multiplying the r scale by the factor $F(h)$, which is plotted in Figure 11*b*.

The beam pattern is shown in Figure 12 for the untapered case (Fig. 12*a*), and for a tapering function $T(\rho) = \exp \{\ln 0.25\, \rho^2/\rho_{max}^2\}$ (Fig. 12*b*). The FWHM is 4'.9 for case *a* and 6'.0 for case *b*, while the level of the first sidelobe is at −25% for case *a* and only −10% of the beam maximum for case *b*.

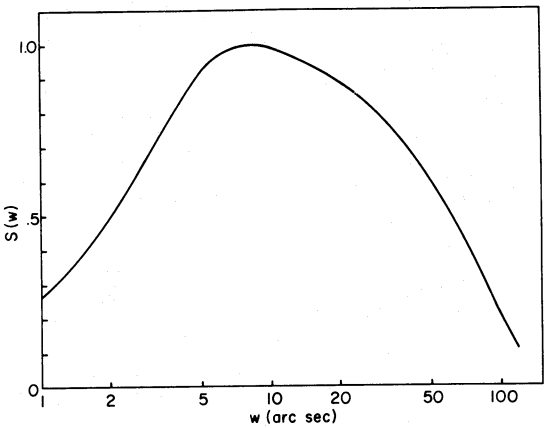

FIG. 13.—Relative sensitivity of one-dimensional synthesis to Gaussian sources with FWHM equal to w, at zero hour angle

A serious problem with interferometers which have regularly spaced dishes is that the beam pattern repeats itself on the sky plane at intervals of $1/\Delta b$ radians, where Δb is the baseline increment. In our case, with $\Delta b =$ 72 m ($=1200\lambda$), this would mean a repetition distance of 2.9, which would have caused considerable difficulty in determining the exact position of a burst source on the Sun. Therefore we placed the movable telescope A at a distance of 90 m from the fixed telescope 9, so that the smallest baseline was $b_{\min} = 90$ m (1500λ) while the baseline increment remained at $\Delta b = 72$ m (1200λ). The repetition distance in this case is the inverse of the largest common divider of $b_{\min}$ and Δb, i.e., 1/300 rad or 11.4 (Fig. 12). We still have grating lobes at distances of 2.9, but these have an entirely distinct shape from the main lobe. To achieve this repetition distance with all spacings being equal, one would need to have $\Delta b = 18$ m (300λ), which would require 4 times more baselines than we had.

Because of the nonzero value of $b_{\min}$, large sources are not detectable. If we ignore the effects of the primary beam, the visibility of a one-dimensional Gaussian source of the form

$$I_1(r) = I_0 \exp(-\ln 16 r^2/w^2) \tag{A9}$$

will be

$$V(\rho) = \frac{\pi}{\ln 16} w I_0 \exp\left(-\frac{\pi^2 w^2 \rho^2}{\ln 16}\right) \tag{A10}$$

while the untapered interferometer response at $r = 0$ will be

$$I_{\text{obs}}(0) = 2\left(\frac{\pi}{\ln 16}\right)^{1/2} w I_0 \sum_{j=1}^{n} \exp\left(-\frac{\pi^2 w^2}{\ln 16} \rho_j^2\right). \tag{A11}$$

If we define a sensitivity as the ratio of the observed to the true intensity of the source, we get

$$S(w) \equiv \frac{I_{\text{obs}}(0)}{I_0} = 2\left(\frac{\pi}{\ln 16}\right)^{1/2} w \sum_{j=1}^{n} \exp\left(-\frac{\pi^2 w^2}{\ln 16} \rho_j^2\right). \tag{A12}$$

A plot of $S(w)$ is shown in Figure 13; the sensitivity drops to less than 50% for sources larger than ~ 1.03 and smaller than $\sim 2''$. If a Gaussian tapering function is used, the source width in equations (11) and (12) should be replaced by $w' = (w^2 + w_t^2)^{1/2}$, where w_t is the taper FWHM.

REFERENCES

Alissandrakis, C. E. 1977, Ph.D. thesis, University of Maryland.
Alissandrakis, C. E., and Kundu, M. R. 1975, *Solar Phys.*, **41**, 119.
Enomé, S., Kakinuma, T., and Tanaka, H. 1969, *Solar Phys.*, **6**, 428.
Felli, M., Pallavicini, R., and Tofani, G. 1975, *Solar Phys.*, **44**, 135.
Hobbs, R. W., Jordan, S. D., Maran, S. P., Caulk, H. H., and Webster, W. J., Jr. 1973, *Ap. Letters*, **15**, 193.
Högbom, J. A., and Brouw, W. N. 1974, *Astr. Ap.*, **33**, 289.
Kahler, S. W., Krieger, A. S., and Vaiana, G. S. 1975, *Ap. J. (Letters)*, **199**, L57.
Kundu, M. R. 1959, *Ann. d'Ap.*, **22**, 1.
———. 1961, *J. Geophys. Res.*, **66**, 4308.
———. 1965, *Solar Radio Astronomy* (New York: Interscience).
Kundu, M. R., and Alissandrakis, C. E. 1975, *Nature*, **257**, 465.
Kundu, M. R., Alissandrakis, C. E., Bregman, J., and Hin, A. C. 1977, *Ap. J.*, **213**, 278.
Kundu, M. R., Alissandrakis, C. E., and Kahler, S. W. 1976, *Solar Phys.*, **50**, 429.
Kundu, M. R., Becker, R. H., and Velusamy, T. 1974, *Solar Phys.*, **34**, 175.
Kundu, M. R., Velusamy, T., and Becker, R. H. 1974, *Solar Phys.*, **34**, 217.
Pallavicini, R., and Vaiana, G. S. 1976, *Solar Phys.*, **49**, 297.
Takakura, T., 1967, *Solar Phys.*, **1**, 304.
Vorpahl, J. A., Gibson, E. G., Landecker, P. D., McKenzie, D. L., and Underwood, J. H. 1975, *Solar Phys.*, **45**, 199.
Weiler, K. W. 1973, *Astr. Ap.*, **26**, 403.

C. E. ALISSANDRAKIS and M. R. KUNDU: Astronomy Program, University of Maryland, College Park, MD 20742